



Failure Modes of Air Desaturated Sand in Undrained Cyclic Loading: A Systematic Experimental Investigation

Dhanaji Chavan¹ · Thallak G. Sitharam¹ · P. Anbazhagan¹

Received: 18 June 2021 / Accepted: 2 November 2021 / Published online: 17 November 2021
© Indian Geotechnical Society 2021

Abstract This paper presents a systematic experimental investigation to understand different failure modes of air desaturated clean sand in undrained cyclic loading for a degree of saturation in the range of 70% to full saturation. Five distinct failure modes have been observed depending on the degree of saturation, relative density, effective confining pressure and cyclic shear stress ratio. Nearly saturated samples of loose sand at low confining pressure underwent hybrid cyclic liquefaction failure wherein it reached dense of critical state during compression stage of loading only. However, nearly saturated samples of medium dense sand at low confining pressure accumulated large plastic strain on the compression side owing to gradual strain softening. Both loose and medium dense samples, with a high degree of saturation, underwent cyclic mobility failure at high effective confining pressure, wherein the sample reached dense of critical state during both compression and extension stage of loading. Moreover, two types of cyclic softening failures, demarcated by two distinct phase transformation trends, were observed in samples with a low degree of saturation. Investigation from the critical state soil mechanics framework revealed that all test samples lay on the dense-of-critical side, and nearly saturated samples closest to critical state underwent cyclic

mobility failure, whereas those at farthest from critical state failed by gradual strain softening.

Keywords Air desaturation · Pore pressure ratio · Initial liquefaction · Double amplitude axial strain · Cyclic mobility

List of Symbols

S	Degree of saturation of the sample
e	Void ratio of the sample
n	Porosity of the soil sample
K_s	Bulk modulus of soil skeleton
K_w	Bulk modulus of water
u_a	Absolute pore fluid pressure
B	Skempton's pore pressure parameter
D_r	Relative density of the sample
N	Number of loading cycles
r_u	Pore pressure ratio
q'	Deviatoric stress
σ'_c	Initial effective confining pressure
σ'_3	Effective minor principal stress
σ'_1	Effective major principal stress
CSR	Cyclic shear stress ratio

✉ Dhanaji Chavan
dschavan83@gmail.com

Thallak G. Sitharam
sitharam@iisc.ac.in

P. Anbazhagan
anbazhagan@iisc.ac.in

¹ Department of Civil Engineering, Indian Institute of Science, Bangalore 560012, India

Introduction

It is a well-established fact that a fully saturated sandy soil, when subjected to undrained cyclic loading, undergoes two different types of failures: (1) flow failure and (2) cyclic mobility [1–5]. However, a recent study by Sze and Yang [6] revealed that a fully saturated clean sandy soil subjected to undrained cyclic loading undergoes three more

additional modes of failure: (1) cyclic plastic strain accumulation, (2) limited flow followed by cyclic mobility and (3) limited flow followed by cyclic plastic strain accumulation; depending upon the method of sample preparation, initial effective confining pressure and initial static shear stress.

Research carried over the last two decades has suggested that in the near future, desaturation of in situ saturated sandy soil can be a possible cost-effective and environment-friendly liquefaction mitigation technique [7–12]. This technique relies on a principle of making pore fluid compressible by either injecting air externally into the soil mass or internally generating some form of gas in the soil body [13, 14].

Some researchers recently conducted centrifuge and shaking table studies and found that induced desaturation suppresses the initial liquefaction of desaturated sandy soil [9, 14, 15]. Studies on shallow footings revealed that when footing subsoil was desaturated, a significant reduction in generation of excess pore pressure and footing settlement happened [10, 12, 16]. It was found from monotonic triaxial tests on microbially desaturated clean sand that even 10% reduction in the degree of saturation doubled the undrained shear strength of the soil [17].

Though noteworthy research has been carried out, on desaturation, most of them are focused on devising desaturation techniques and/or quantifying increase in the liquefaction resistance due to desaturation. A study to understand failure modes of such soil under undrained cyclic loading is yet to be carried out. In this study, a large number of stress-controlled undrained cyclic triaxial tests have been conducted to investigate the effect of air desaturation on failure modes of triaxial specimens. The degree of saturation of tested samples varied from 70 to 99%. Relative density of samples was 30%, 40% and 60%. Effective confining pressure employed in present study was 25 kPa, 50 kPa and 100 kPa. The sinusoidal cyclic load was applied at a frequency of 0.1 Hz. The cyclic shear stress ratio (*CSR*) was 0.25 unless otherwise specified.

The setup for cyclic triaxial machine used in this study is shown in Fig. 1. The displacement transducer (LVDT) can measure displacement up to 100 mm and has the least count of 0.01 mm; the load cell has the capacity of 500 kg, and its least count is 0.1 kg. Cell pressure and pore pressure transducers have the capacity of 1000 kPa with the least count of 1 kPa.

Material and Methods

Clean sand passing through 2 mm IS sieve and retained on 0.075 mm IS sieve has been used in this study. The index properties of the sand have been determined following the

appropriate Indian Standards [18–20] and are given in Table 1. As per IS soil classification system, it is a poorly graded fine sand.

Sample Preparation

Cylindrical samples of diameter 50 mm and height 100 mm were prepared using the dry deposition method. It is worth to note that this is one of the most widely used specimen preparation methods [3, 6, 21].

In this method, a latex rubber membrane is lined against the inner surface of the split mould, and a predetermined mass of oven-dry sand is deposited in five layers. Sand mass is deposited through a funnel with the spout at zero drop height. Little tamping is done with the spout tip at the end of each layer. Once the fifth layer is deposited, little tamping and side taping is done. Then, the vacuum of 10 kPa is applied to the sample and the split mould is removed. Applied vacuum induces effective confining pressure of 10 kPa, which imparts rigidity to the sample, owing to which sample retains its shape and size even after removal of split mould. Then cell is filled with water, and vacuum is slowly reduced to zero; at the same time, cell pressure is increased from 0 to 10 kPa. Thus, effective confining pressure of 10 kPa is maintained throughout. This was followed by sample saturation. It should be noted that specimens of different relative densities were prepared by depositing different quantities of the dry sand mass. The mass of dry sand to be deposited in the split mould for given relative density was computed employing a mass–volume relationship. The drop height was maintained to be zero for all relative densities, and compaction effort, i.e. tamping, was increased to achieve higher relative density.

Saturation of the Sample

Once the sample was prepared, CO₂ gas was passed in two stages: (a) under a vacuum of 10 kPa for 10 min, (b) without vacuum for the next 20 min (total 30 min), followed by percolation of 1000 ml of distilled water. Then Skempton's *B* parameter was measured and was found to be 0.8. It should be noted that *B* parameter of 0.8 at zero back pressure corresponds to a degree of saturation as high as 99% as shown in Fig. 2. Moreover, according to Black and Lee [22] a sample with the degree of saturation of 99% can be considered a fully saturated sample from the practical point of view.

Computation of the Degree of Saturation (*S*)

As the present study focuses on desaturated sandy soil, in which pore fluid comprises air–water mixture, it is essential to quantify the degree of saturation of the sample as

Fig. 1 Photographic view of cyclic triaxial setup used in present study

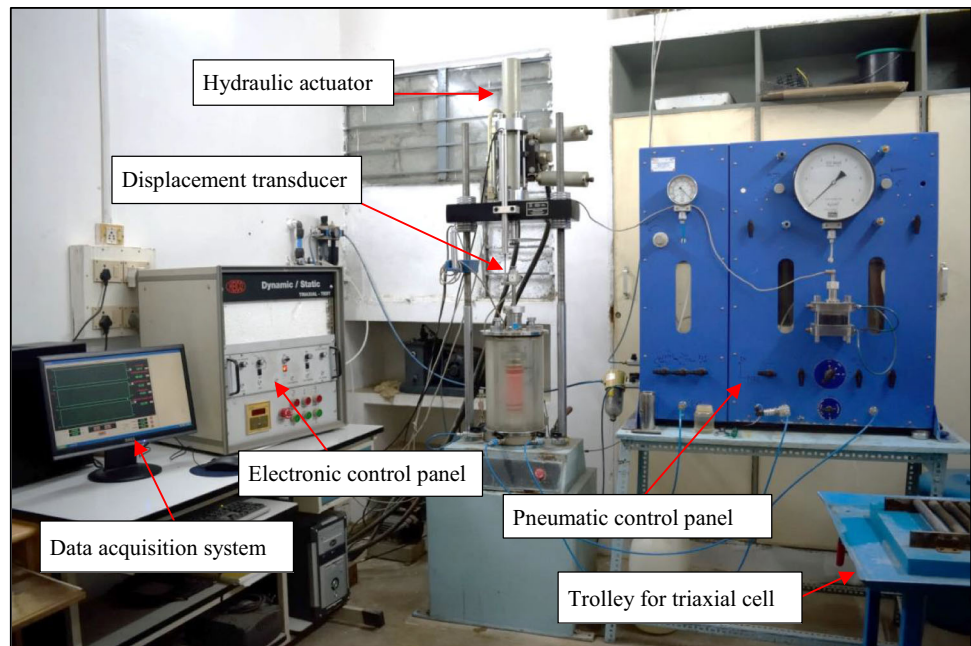


Table 1 Index properties of the sand used in the present study

Specific gravity (G)	e_{\max}	e_{\min}	ρ_{\max} (gm/cc)	ρ_{\min} (gm/cc)	D_{10} (mm)	D_{30} (mm)	D_{50} (mm)	D_{60} (mm)	C_u	C_c
2.65	0.84	0.45	1.83	1.44	0.14	0.20	0.27	0.30	2.14	0.95

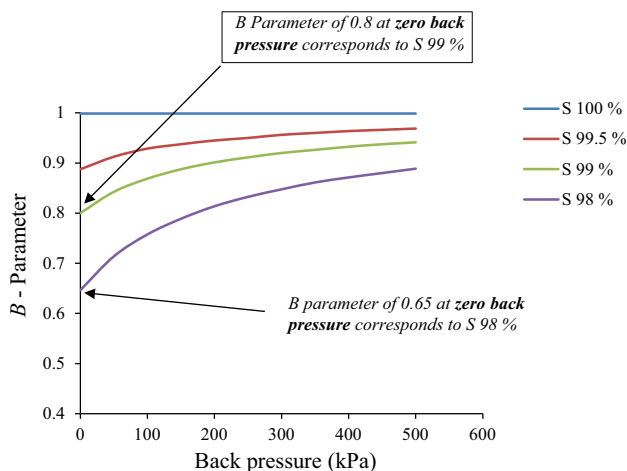


Fig. 2 Back pressure dependency of B parameter at S less than 100% (D_r , 30%)

accurately as possible. Conventionally, the saturation of the sample is assessed by measuring Skempton’s pore pressure parameter B [23]. It is worthy to note here that in the case of the fully saturated sample, B parameter is independent of the backpressure, whereas in the case of the partly saturated sample, it depends upon the back pressure at which it is measured. This fact is very much clear from Eq. (1)

given below, which is widely used to compute the degree of saturation of a partly saturated sample [24, 25].

$$B = \frac{1}{1 + nK_s[S/K_w + (1 - S)/u_a]} \quad (1)$$

where u_a is the absolute pore fluid pressure (i.e. atmospheric pressure + back pressure + Δu) at the end of cell pressure increment $\Delta\sigma_c$ [26], atmospheric pressure is 101.3 kPa, Δu is the increase in pore water pressure when cell pressure increment of $\Delta\sigma_c$ is applied, S is the degree of saturation of the sample, n is the porosity of the sample, K_s is the bulk modulus of the soil skeleton, and K_w is the bulk modulus of the pore water which has a standard value of 2.23×10^6 kPa. Porosity n was computed from the void ratio of the sample, which was computed from the relative density of the sample, and bulk modulus of the soil skeleton K_s was determined from the isotropic compression of the saturated sample [26].

From Eq. (1), it is clear that for given S , other than $S = 1$, the value of B parameter varies with back pressure. This variation of B parameter with back pressure is shown in Fig. 2. It is observed that for a degree of saturation of 99.5%, B parameter is 0.89 at zero back pressure and 0.97 at 500 kPa back pressure. In other words, B parameter of 0.89 at zero back pressure is equivalent to B parameter of

0.97 at 500 kPa back pressure. This means that in the case of a partly saturated sample degree of saturation computed from Eq. (1) is function of both B parameter and corresponding back pressure. Similarly, for a degree of saturation of 99.0%, these values are 0.80 and 0.94, respectively. Thus, even a small reduction in the degree of saturation below full saturation causes a significant reduction in B parameter. It is also clear from Fig. 2 that for significantly higher degrees of saturation, the B parameter increases with an increase in back pressure till a certain limiting value of back pressure and then attains a constant value. It should be noted that in the present study, samples were saturated and desaturated at zero back pressure. The relationship between B parameter and degree of saturation, used in this study, at zero back pressure is given in Fig. 3. It should be noted that in this study, B parameter was measured during saturation and after desaturation. Then using Eq. (1), the degree of saturation of the sample was computed.

Desaturation of the Sample

The back pressure pipe was disconnected from the triaxial cell, and a pipe supplying air was connected at this place as shown in Fig. 4. Then air was injected into the sample under very small pressure of around 1 to 2 kPa. During air injection, the drainage valve was kept open to collect the water pushed out by injected air. Different quantities of water got ejected depending on the time for which air injection was continued. Thus, different degrees of saturation were achieved by ejecting different quantities of water. Once air injection was over, the air supply pipe was disconnected from the triaxial cell, and the back pressure pipe full of water was connected back. The back pressure pipe was kept connected in this way for 10 min under a

pressure of around 1 to 2 kPa. Then B parameter of the desaturated sample was measured, and the degree of saturation was computed using Eq. (1).

It should be noted here that initial pore water pressure in the specimen was just equal to hydrostatic pressure, as samples were saturated at zero back pressure as mentioned in previous section. The hydrostatic pressure at the base of the sample was just 1 kPa (i.e. 0.1 m height \times 9.81). It was suggested by Ishihara et al. [7], from their centrifuge studies that to inject the air into the saturated soil mass, the air injection pressure at the injection point has to be around 1.4 times the hydrostatic pressure at that point.

To assess uniform distribution of the injected air in the specimen, post-desaturation water content determination of the specimen was carried out. The water content was determined at top, middle and bottom of the specimen. The water content measured at these three locations was in reasonable agreement. This ensures the almost uniform distribution of the injected air in the specimen. Five such tests were conducted at the beginning of the research. Further, volume change of the sample was not monitored during desaturation. This is so because the volume of pushed out water was being replaced with the volume of the injected air. Therefore, volume change, if any, during desaturation was assumed to be negligible.

Results and Discussion

Issues such as effect of initial effective confining pressure and relative density on the failure mode, failure modes at a low degree of saturation, cyclic mobility versus cyclic softening and liquefaction failure criteria have been discussed in detail in the following sections.

It is essential to understand the following terminologies for understanding results from this study: (a) *Compression stage of loading*: axial stress is increased above initial effective confining pressure to a predefined value. (b) *Extension stage of loading*: axial stress is decreased below initial effective confining pressure to a predefined value. (c) *Extension*: increase in the height of the specimen. (d) *Compression*: decrease in the height of the specimen. (e) *Contraction*: decrease in volume of the specimen. (f) *Dilation*: increase in the volume of the specimen. (g) *Pore pressure ratio (r_u)*: It is the ratio of excess pore pressure to initial effective confining pressure. (h) *Initial liquefaction*: a state at which r_u is 1, i.e. a state at which effective confining pressure acting on the sample is zero.

Effect of Initial Effective Confining Pressure (σ'_c)

This section discusses cyclic response of nearly saturated samples (S 98.5%) and samples with S around 90%.

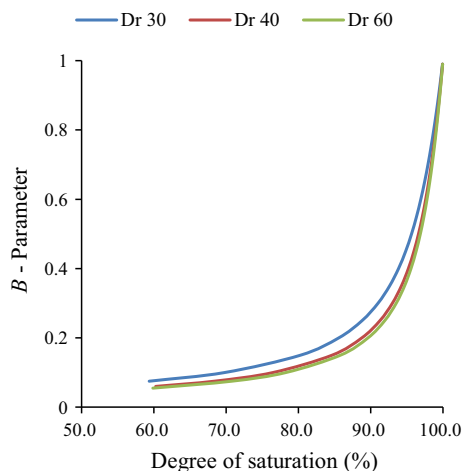
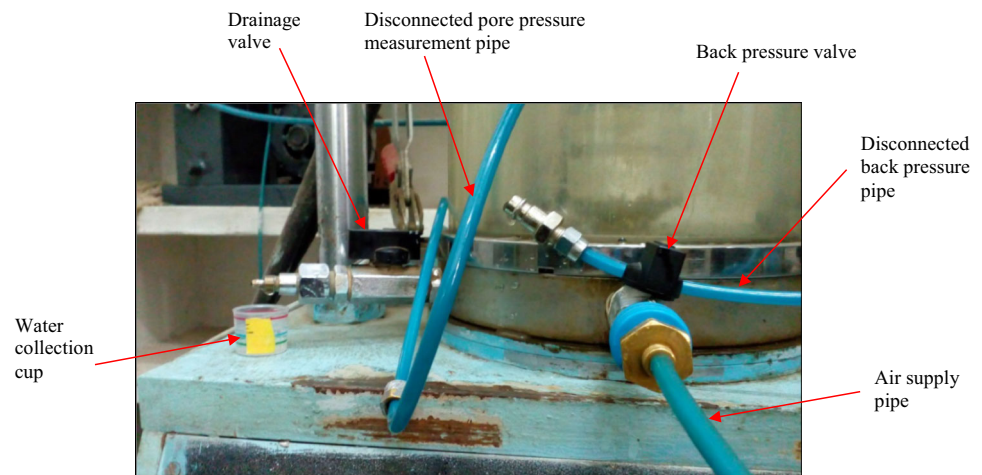


Fig. 3 Relationship between degree of saturation and B parameter for sand used in this study

Fig. 4 Connection details during air injection



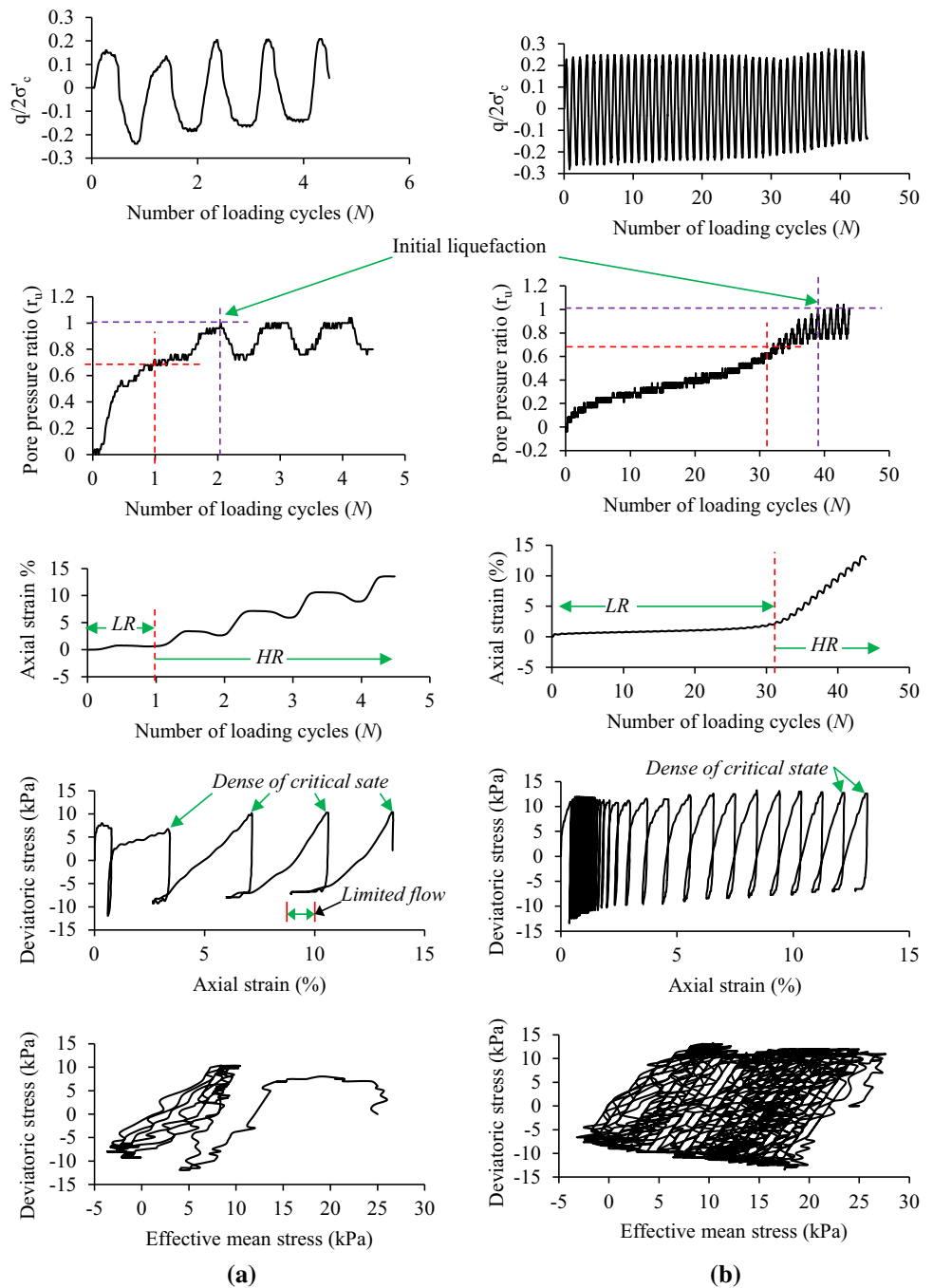
Response of samples with a lower degree of saturation is discussed elsewhere. Cyclic response of samples, at initial effective confining pressure (σ'_c) of 25 kPa, for relative density (D_r) of 30%, 40% and 60% is shown in Figs. 5, 6 and 7, respectively. From Fig. 5, it is clear that in the case of D_r 30%, both nearly saturated sample (S 98.5%) and sample with S of 87.2% fail by accumulating plastic strain on the compression side. Both pore pressure ratio evolution and axial strain evolution are faster in the nearly saturated sample than those in the sample with S of 87.2%. Further, in the case of S 98.5% sample reaches initial liquefaction at the end of 2nd cycle. After reaching the initial liquefaction, the sample undergoes large axial straining during the compression stage of loading followed by a stable state in each consecutive loading cycle, as shown in Fig. 5a. The stable state achieved at the end of large axial straining is given by sharp peaks observed in the stress strain curve. This stable state, after initial liquefaction, is called as dense of critical state [5]. However, during the extension stage of loading sample undergoes limited flow, as shown in Fig. 5a, and no sharp peaks similar to the compression stage of loading are observed. In limited flow, the sample undergoes limited axial straining at constant deviatoric stress as observed in Fig. 5a. This type of response is called as “hybrid cyclic liquefaction”.

The axial strain evolution for S 98.5% and S 87.2% has two distinct parts: (1) evolution of axial strain with low rate (LR) (2) evolution of axial strain with high rate (HR) as shown in Fig. 5. It is the pore pressure ratio (r_u) which defines the transition from LR to HR. From Fig. 5, it is observed that, in both cases, the transition happens at pore pressure ratio (r_u) of around 0.6. For D_r 40% also both nearly saturated sample (S 98.5%) and sample with S of 90% fail by hybrid cyclic liquefaction as seen in Fig. 6. It should be noted that in the case of S 90%, sample undergoes little extension before undergoing significantly large compression as seen in Fig. 6b.

In the case of D_r 60%, nearly saturated sample (S 98.5%) accumulated plastic strain at a very slow rate, as seen in Fig. 7a. With the evolution of pore pressure, it underwent gradual strain softening. In strain softening, there is a reduction in the stiffness of the sample. This stiffness reduction results in relatively large axial straining during consequent loading cycles as observed in Fig. 7a. Sample reached pore pressure ratio (r_u) of 1 at the end of 204 cycles; corresponding axial strain was 8.76%. The axial strain at the end 206 cycles became 9.51%. Thus, even though the sample attained r_u of 1, it did not undergo sudden and large axial straining, which is observed in typical liquefaction failures. Therefore, such failure cannot be called as liquefaction failure even though the sample reached r_u of 1. In this paper, this failure is named as FAPSCS-SS: failure due to accumulation of plastic strain on compression side as a result of gradual strain softening. In the case of the sample with S 94.9% and D_r 60%, the axial strain accumulated at the end of 258 cycles was just 0.64%, and the maximum pore pressure ratio was just 0.44 as seen in Fig. 7b. The axial strain evolution of nearly saturated samples of D_r 30%, 40% and 60% is shown in Fig. 8. From this figure, it is clear that in the case of hybrid cyclic liquefaction, observed in D_r 30% and D_r 40%, there is a sudden increase in the axial strain due to sudden buildup of high pore pressure, whereas in the case of FAPSCS-SS, axial strain evolution is gradual and at a very slow rate.

The response of samples with a relative density of 30%, at σ'_c of 100 kPa is shown in Fig. 9. From this figure, it is observed that samples with S 98.5% and S 89.2% underwent cyclic mobility. Peaks in stress–strain curves are an indication of dense of critical state reached during compression and extension stage of loading. Further, samples with D_r 40% and 60% also underwent cyclic mobility failure, as shown in Fig. 10. In this figure, for brevity, stress–strain curve and effective stress path only are shown.

Fig. 5 Hybrid cyclic liquefaction failure of samples of D_r 30% at σ'_c 25 kPa: **a** S 98.5, B 0.7% **b** S 87.2%, B 0.21

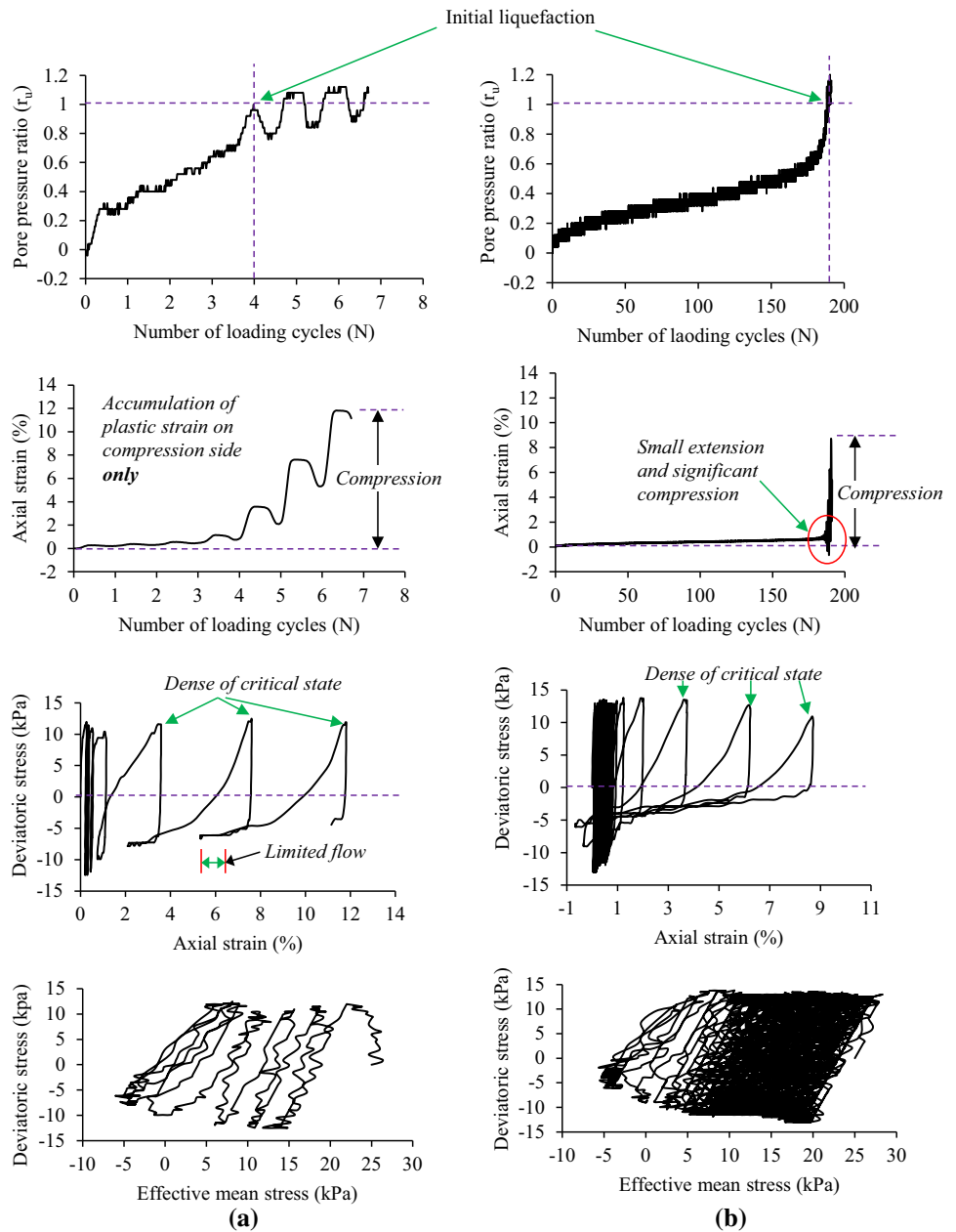


It is worth to note that samples of D_r 30% and 40% with S around 90% show smoothed peaks on the extension side, as seen in Figs. 9 and 10.

In the case of smoothed peaks, the sample attained dense of critical state at a slower rate than its nearly saturated counterpart. This resulted in relatively large axial straining of such samples. The stress–strain curves shown in Figs. 9 and 10 support this interpretation. In Fig. 9, over the last two cycles, a nearly saturated sample of D_r 30% strained from -7 to -10.5% , i.e. net axial straining of

3.5% whereas sample with S 89.2% strained from -7 to -13% , i.e. net axial straining of 6% . Similarly, in the case of D_r 40%, nearly saturated sample strains from -2 to -9% , i.e. net axial straining of 7% , whereas sample with S 89.2% strains from -10 to -18% , i.e. net axial straining of $8\% > 7\%$, indicating relatively large deformation required to reach a dense of the critical state.

Fig. 6 Hybrid cyclic liquefaction failure of samples of D_r 40% at σ'_c of 25 kPa: **a** S 98.5%, B 0.65 **b** S 90%, B 0.20



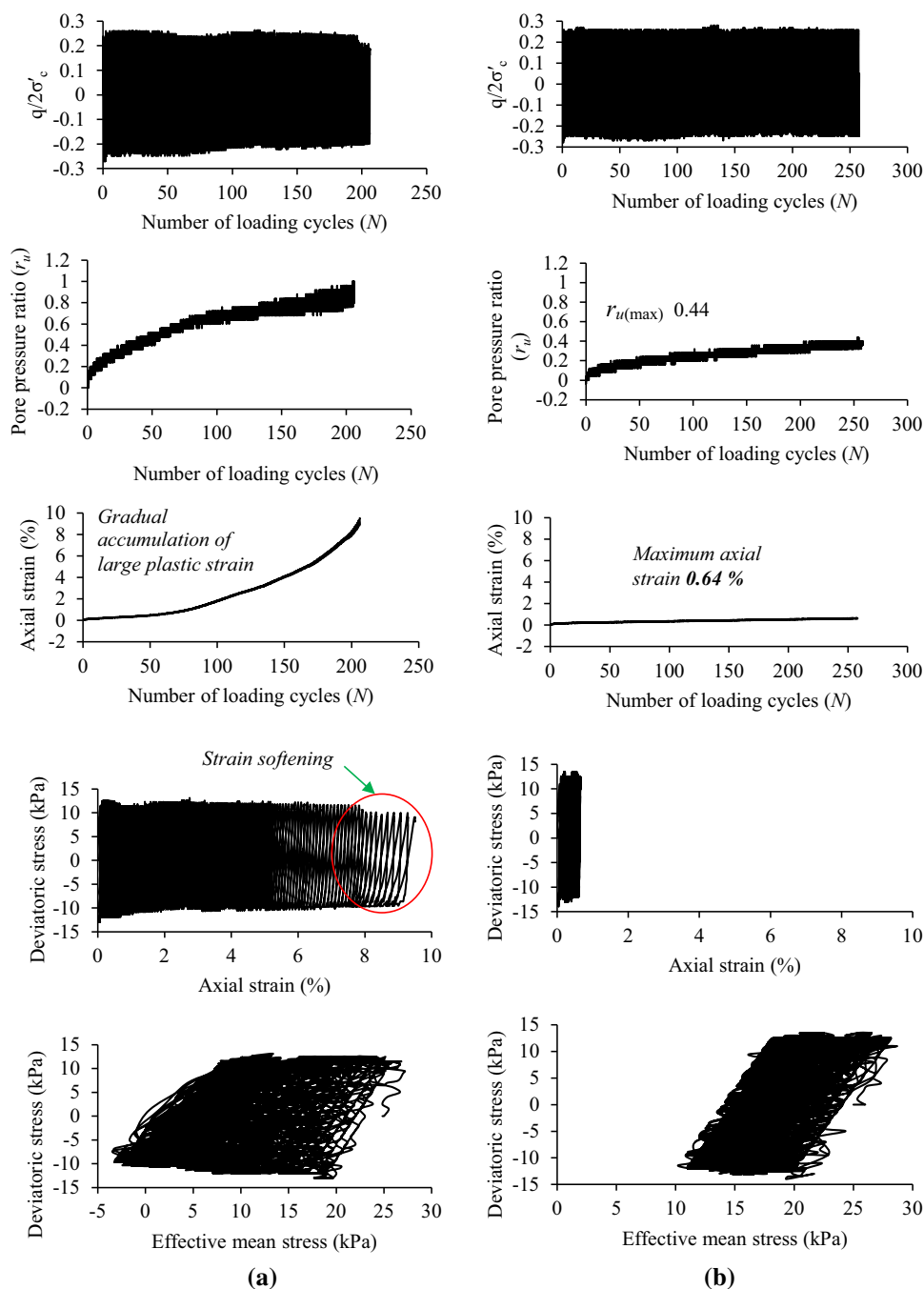
Effect of Relative Density (D_r)

From Figs. 5, 6, 7, it is observed that nearly saturated samples and samples with S around 90% of loose sand, i.e. D_r 30% and 40%, underwent hybrid cyclic liquefaction failure at an initial effective confining pressure of 25 kPa, whereas nearly saturated sample of medium dense sand, i.e. D_r 60%, underwent FAPSCS-SS failure. At initial effective confining pressure of 100 kPa, both nearly saturated sample and sample with S around 90% underwent cyclic mobility failure, irrespective of the relative density of the sample. However, the cyclic mobility observed at σ'_c 100 kPa can be divided into two categories as: (1)

catastrophic cyclic mobility and (2) gradual cyclic mobility. This has been explained in detail in the following paragraph with the help of Fig. 11.

From Fig. 11, it is clear that nearly saturated samples (S 98.5%) of relative density of 40% and 60% undergo “cyclic mobility” failure. However, pore pressure generation and axial straining are catastrophic in the case of D_r 40%. The pore pressure ratio (r_u) at the end of 0.5th cycle is just 0.1 in the case of D_r 40%. Over the next one cycle, it drastically increases to 0.98, as seen in Fig. 11a. The double amplitude axial strain (DA) over this cycle is 5.50%. In the case of D_r 60%, a pore pressure ratio (r_u) of 0.1 is attained at the end of 1st cycle, and it increases to

Fig. 7 Response of samples of D_r 60% at σ'_c of 25 kPa: **a** S 98.5%, B 0.63 **b** S 94.9%, B 0.32



0.16 over the next one cycle. The double amplitude axial strain (DA) over this cycle is just 0.15%. The practical implication of this finding is that during cyclic loading, generation of even a very small pore pressure ratio of 0.1 can be alarming for loose sand, whereas at the same pore pressure ratio, medium dense sand can be quite stable.

Further, the transition of failure from hybrid cyclic liquefaction to typical cyclic mobility, over low confining pressure to high confining pressure, has been shown in Fig. 12 for a sample of relative density (D_r) of 30%. It is

observed from Fig. 12 that at low initial effective confining pressure, the sample has a tendency to accumulate large strains on the compression side, whereas at high initial effective confining pressure, it undergoes large straining on both compression and extension sides. For other two relative densities, a similar kind of transition is observed but not shown here for brevity.

Few tests were conducted on fully saturated samples, i.e. S 99% [22], as well to see if there is any difference in failure modes of the nearly saturated sample (S 98.5%) and

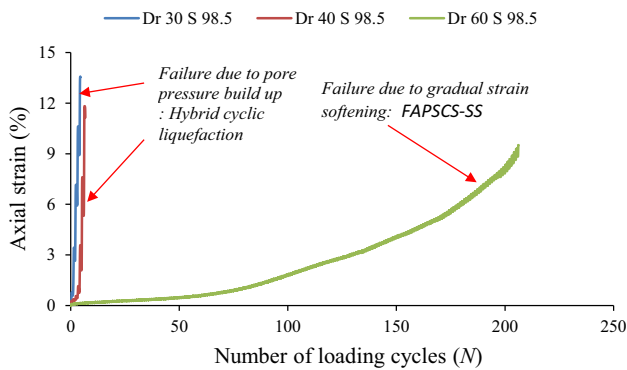


Fig. 8 Comparison of axial strain evolution of nearly saturated sample at different relative densities at confining pressure of 25 kPa

fully saturated sample (S 99%). It is observed that both samples undergo the same failure mode. However, the evolution of pore pressure and axial strain is relatively faster in the fully saturated sample. One such comparison is shown in Fig. 13.

Failure of Desaturated Sample at Low Degree of Saturation

Failure of a sample with a low degree of saturation (S 74%) of relative density of 30% at initial effective confining pressure (σ'_c) of 100 kPa is shown in Fig. 14. It is observed that the sample underwent very large axial straining, i.e. double amplitude axial strain 21.26%, owing to the generation of significantly high pore pressure, i.e. r_u 0.95. Though this pore pressure ratio is less than 1, significantly high pore pressure reduced effective confining pressure, which in turn reduced stiffness and caused large axial deformation. Further, the sample underwent phase transformation over the last few loading cycles during both the compression and extension stages of loading. The phase transformation line on the compression side is named as PTL-C, and that on the extension side is named as PTL-E. This particular type of failure is herein referred to as cyclic softening-CE. Samples of relative density of 40% and σ'_c 100 kPa, with low degree of saturation, exhibited similar kind of responses.

However, in the case of relative density of 60%, the sample with S of 82.1% did not liquefy even at the end of 202 cycles. The maximum pore pressure ratio and axial strain observed, in this case, were just 0.12 and 0.22%, respectively, as shown in Fig. 15.

Response at Higher CSR

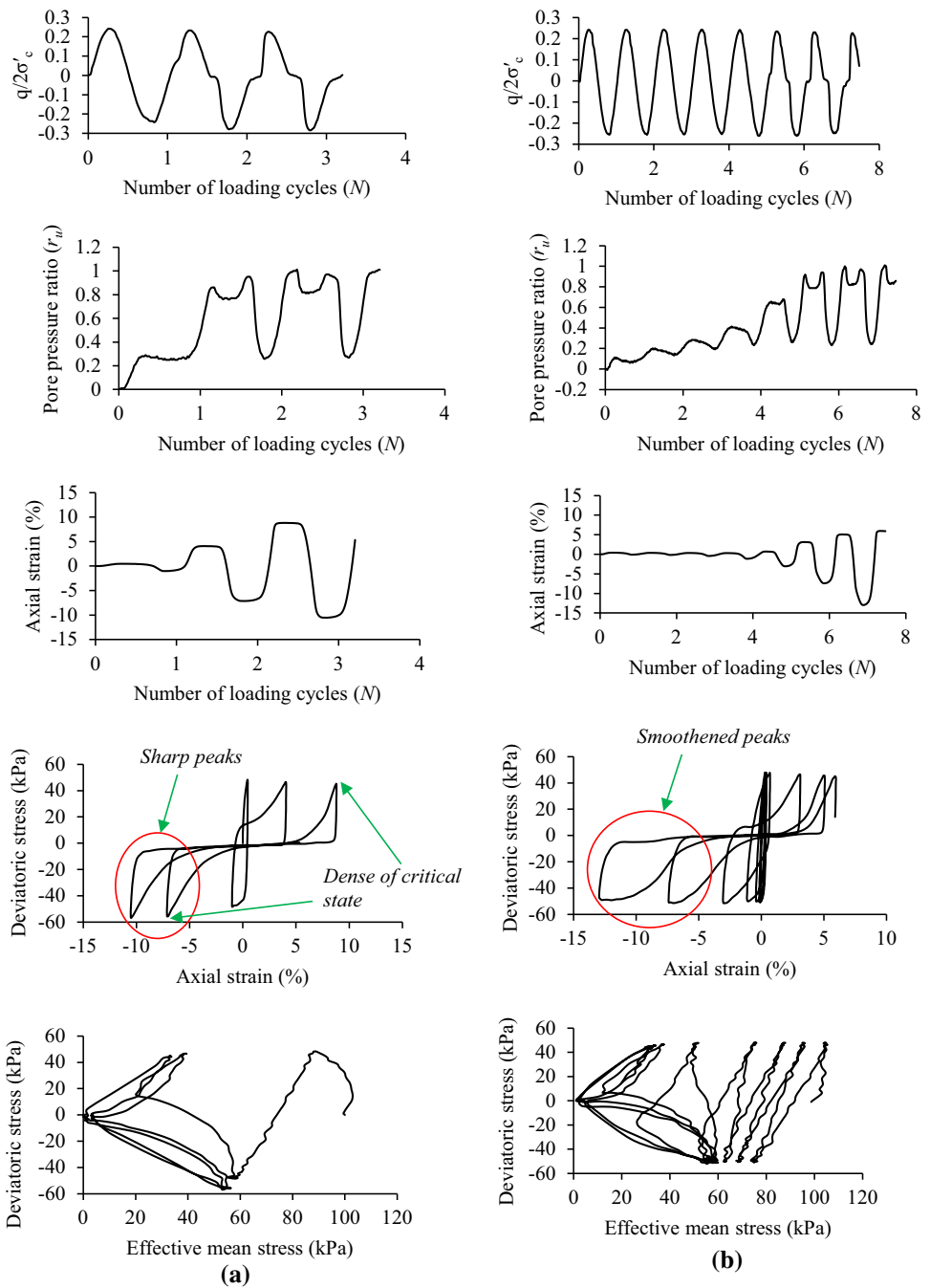
Cyclic response of a nearly saturated and desaturated sample of relative density of 60% under CSR of 0.4 and σ'_c of 100 kPa is shown in Fig. 16. It is observed that nearly

saturated samples underwent cyclic mobility failure, whereas desaturated samples with S 83.6% failed by cyclic softening. However, cyclic softening observed here undergoes phase transformation only during the extension stage of loading, as seen in Fig. 16b. Therefore, herein, this type of failure is entitled cyclic softening-E. Further, the maximum pore pressure ratio developed was 0.46. It is worth to note that in this case, the sample underwent large deformation due to the combined effect of pore water pressure and relatively high cyclic loading, i.e. CSR . This implies that the sample can undergo large deformation even at relatively low pore water pressure when the cyclic load is large.

Importance of Phase Transformation Line and Effective Stress Path

When the sample is subjected to cyclic loading, it may undergo phase transformation during the compression and/or extension stages of loading. When phase transformation happens, there is a sudden reduction in the pore water pressure due to the dilative tendency of the sample. If the sample undergoes phase transformation during the compression stage of loading, it can be identified from the plot of the pore pressure ratio. However, when the sample undergoes dilative tendency during the extension stage of loading, this cannot be identified just from the plot of pore pressure ratio. This is so because pore pressure reduces due to a reduction in the axial stress during the extension stage, even though the sample did not undergo dilative tendency. Moreover, if dilative tendency occurs, then the reduction in pore pressure due to dilative tendency adds to the reduction in pore pressure due to a reduction in axial stress. The phase transformation line tells if the reduction in pore pressure ratio during the extension stage of loading is due to just reduction in axial stress or because of both dilative tendency and reduction in axial stress. This can be explained with the help of Fig. 17. From Fig. 17a and b, it is clear that during cyclic mobility, a phase transformation line is present during both the compression and extension stages of loading. Therefore, reduction in pore pressure ratio during the extension stage of loading is due to: (1) reduction in axial stress and (2) dilative tendency. However, in cyclic softening-E, shown in Fig. 17c and d, the phase transformation line is present on the compression side of loading only and is absent on the extension side. This implies that in this case, reduction in pore water pressure during the extension stage is owing to reduction in axial stress only.

Fig. 9 Cyclic mobility response observed at σ'_c 100 kPa for D_r 30%: **a** S 98.5%, B 0.7
b S 89.2%, B 0.23



Comparison of Stress–Strain Response

Typical stress–strain curves for five failure modes are shown in Fig. 18. It is observed that each stress strain curve is distinct from the other. Cyclic mobility shows a middle nearly flat portion AB, at nearly zero deviatoric stress, along which significant axial straining takes place and stress–strain curve moves from compression side to extension side and vice versa. It is worth to note that when the sample undergoes large axial straining along AB, it changes its phase from contractive to dilative at the end of

the respective loading stage. Due to dilative tendency, there is a reduction in the pore pressure, which causes an increase in stiffness of the sample. This increase in stiffness raises the stress–strain curve to sharp peaks, as seen in Fig. 18b. Sharp peaks are indicators of a stable state owing to dilative tendency.

The middle flat portion AB, which is available in cyclic mobility, is absent in rest four failure modes. In hybrid cyclic liquefaction, sharp peaks similar to those observed in cyclic mobility are observed on the compression side. However, no such peaks are observed on the extension

Fig. 10 Cyclic mobility response observed at σ'_c 100 kPa: **a** D_r 40%, **b** D_r 60%

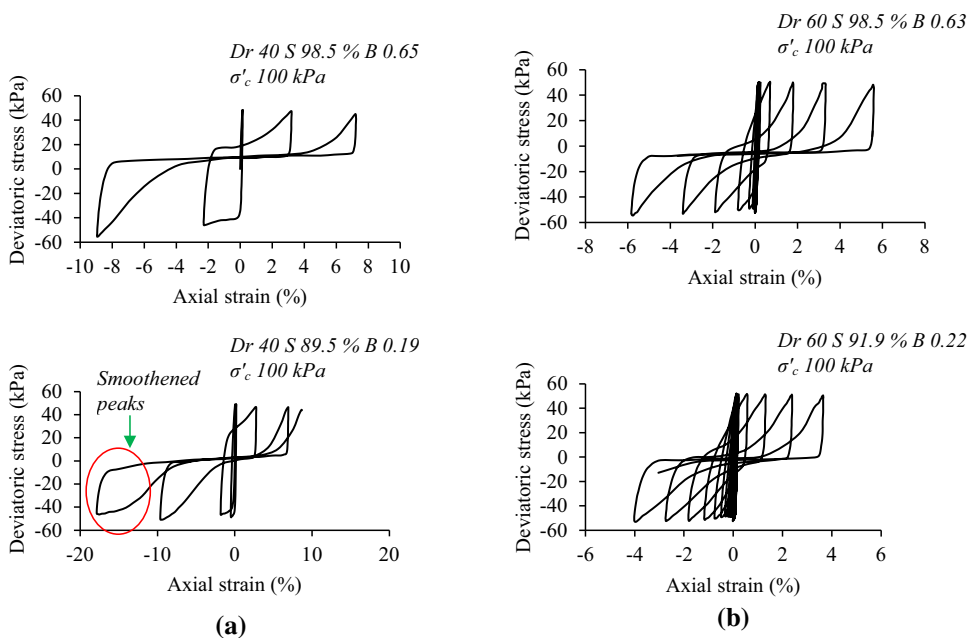
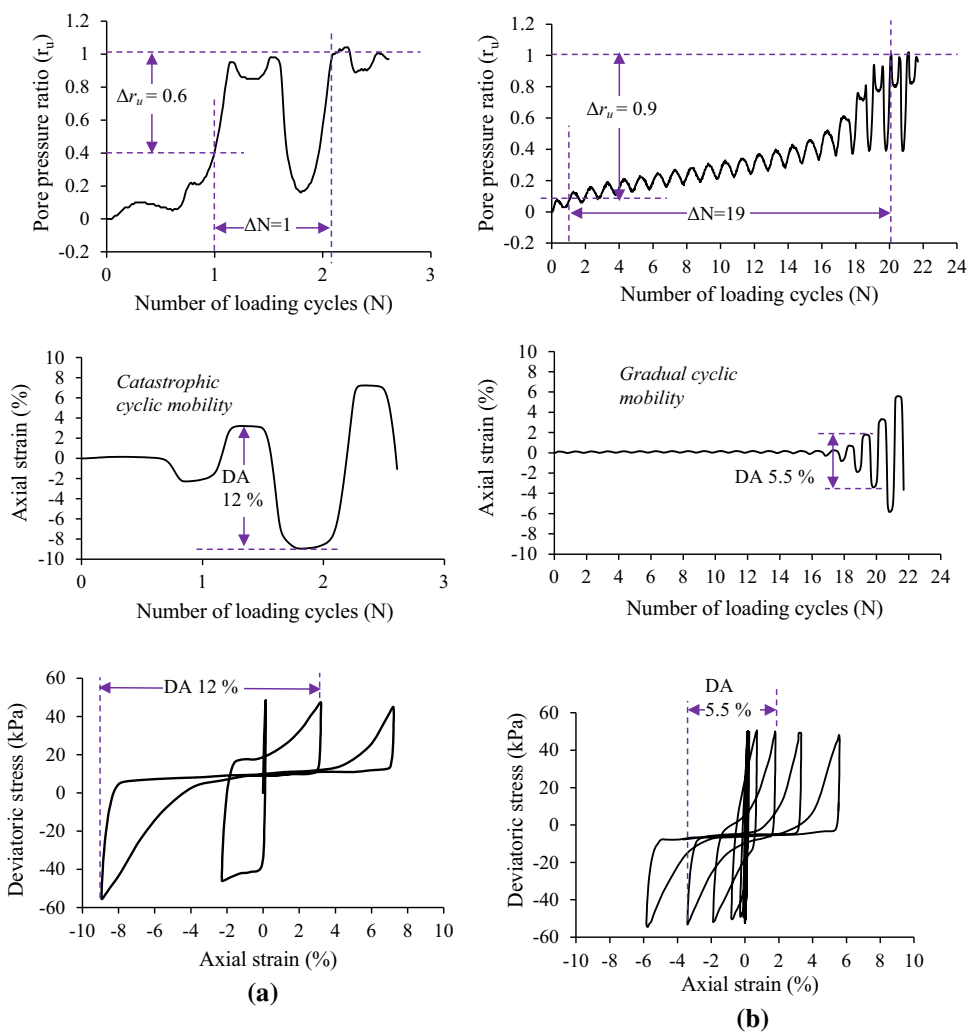


Fig. 11 Catastrophic cyclic mobility and gradual cyclic mobility observed in nearly saturated samples (S 98.5) at σ'_c 100 kPa: **a** D_r 40%, B 0.65 **b** D_r 60%, B 0.63



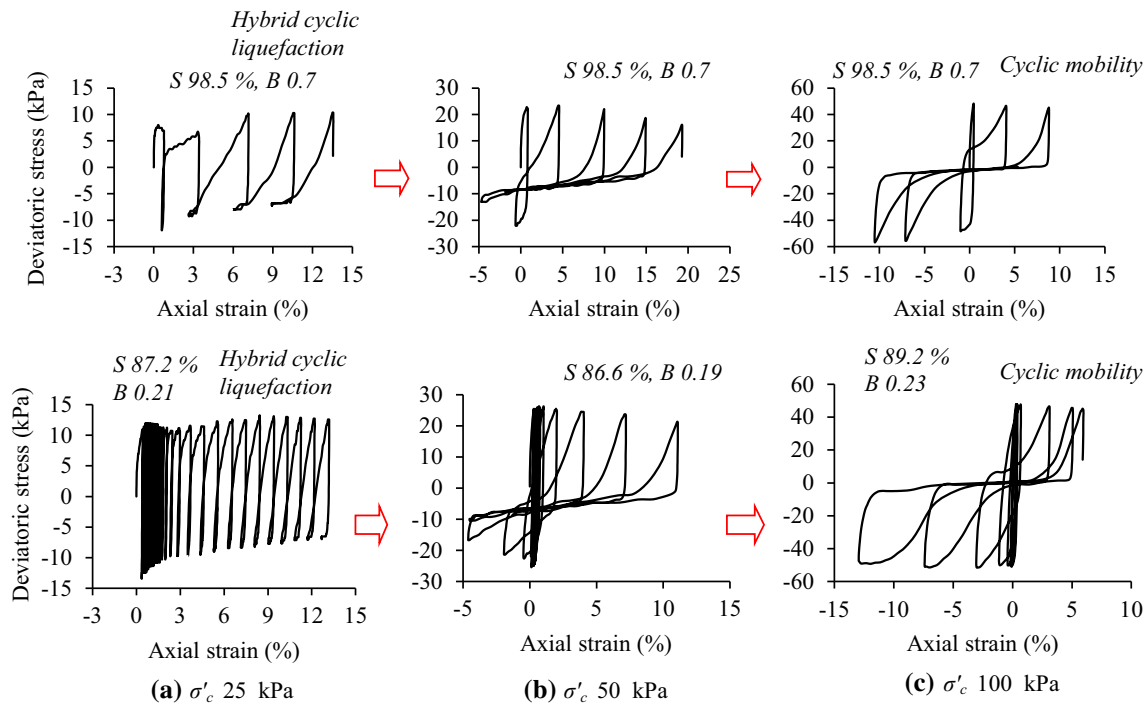
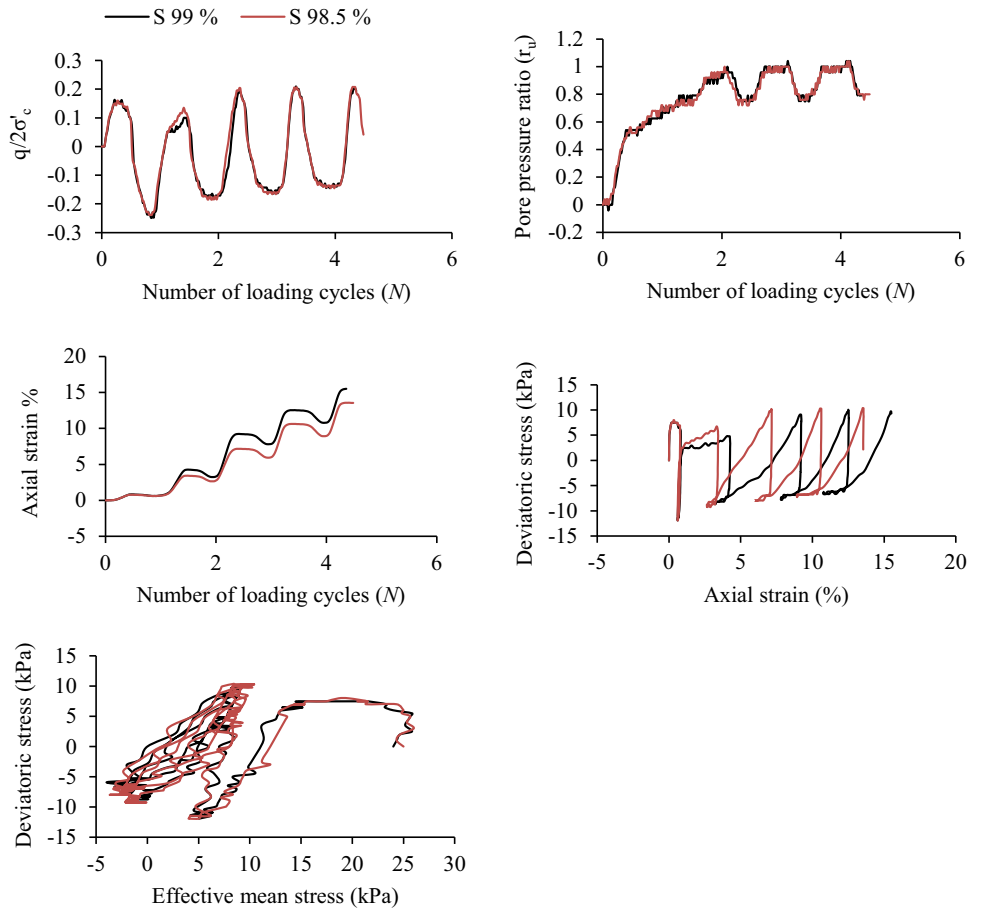


Fig. 12 Transition of stress strain response, for D_r 30%, from “hybrid cyclic liquefaction” to “cyclic mobility” as a function of initial effective confining pressure

Fig. 13 Comparison between cyclic response of saturated (S 99%, B 0.79) and nearly saturated sample (S 98.5%, B 0.7) of D_r 30% at σ'_c 25 kPa



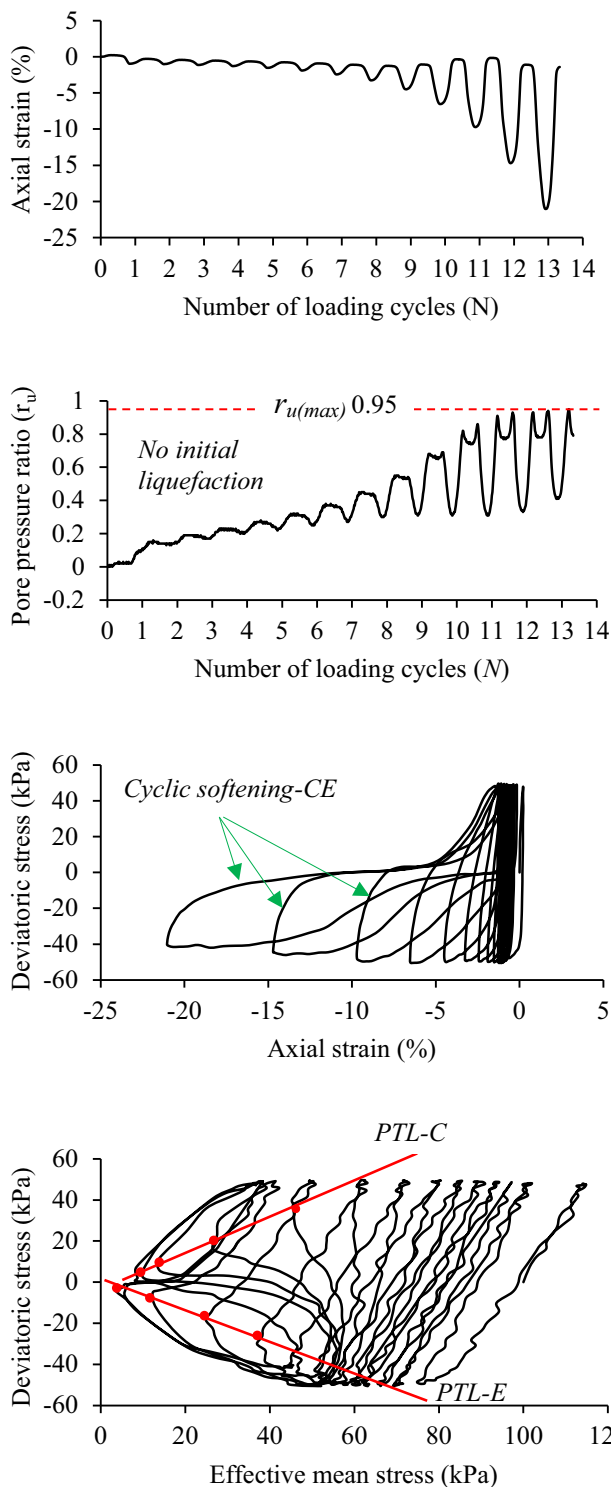


Fig. 14 Cyclic softening-CE of a sample at low degree of saturation (S 74%, B 0.11) of D_r 30% at σ'_c 100 kPa

side. Further, in this failure mode, when the sample moves from the compression stage of loading to the extension stage, the axial strain is constant along the line MN. This peculiar behaviour distinguishes it from typical cyclic

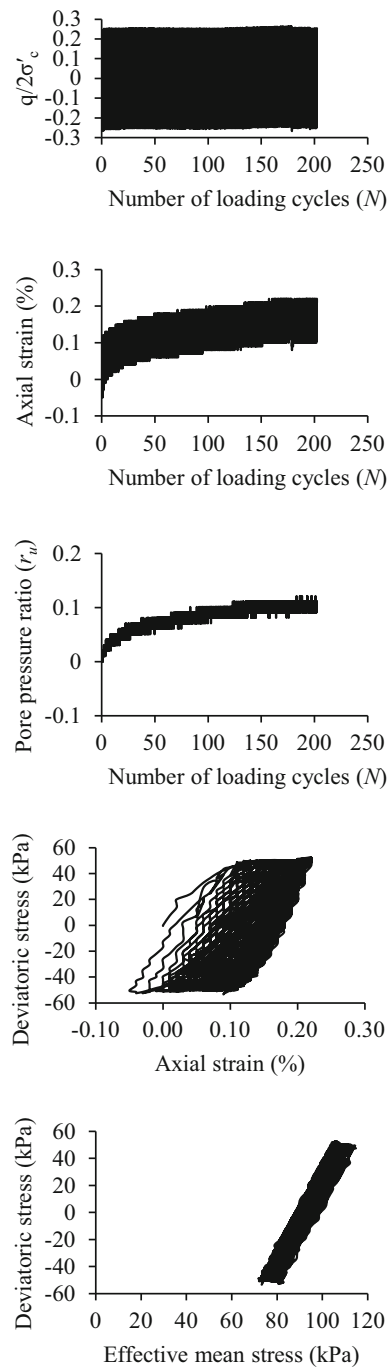
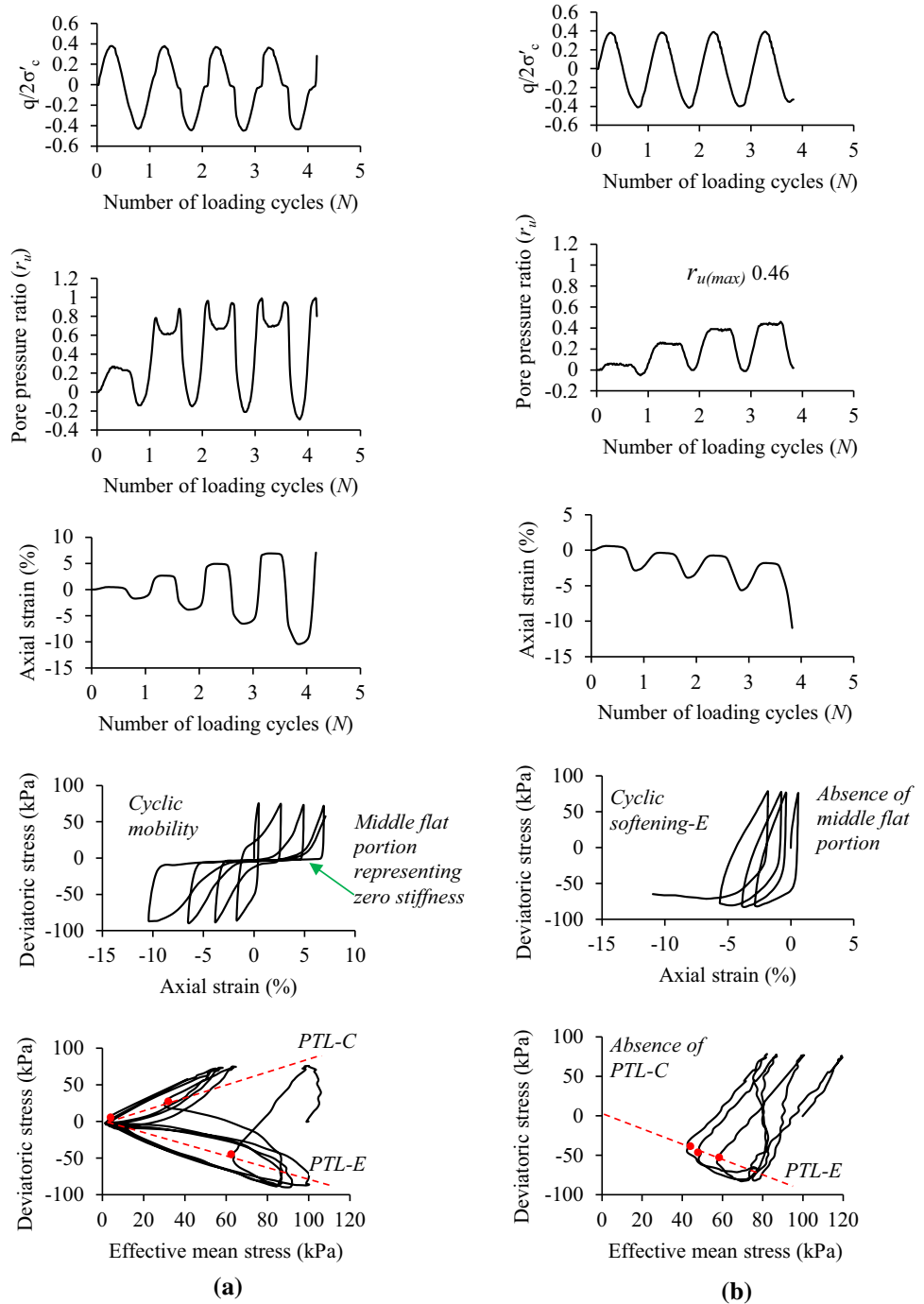


Fig. 15 Response of a sample with S 82.1%, B 0.11 of D_r 60% at σ'_c 100 kPa

mobility failure where axial strain undergoes a significant change at nearly zero deviatoric stress. The constant straining along MN is followed by the limited flow. Limited flow is a phenomenon where the sample undergoes limited axial straining at constant deviatoric stress, as observed in Fig. 18a. This point onward, in a consecutive loading cycle, the sample shows a response which is a combination of sharp peaks on the compression side

Fig. 16 Cyclic mobility and cyclic softening observed at CSR 0.4 for D_r 60% at σ'_c 100 kPa: **a** Cyclic mobility S 98.5%, B 0.63, **b** cyclic softening S 83.6%, B 0.12



similar to cyclic mobility and limited flow on the extension side. This type of response is called as hybrid cyclic liquefaction, as it combines, up to some extent, response of cyclic mobility and limited flow.

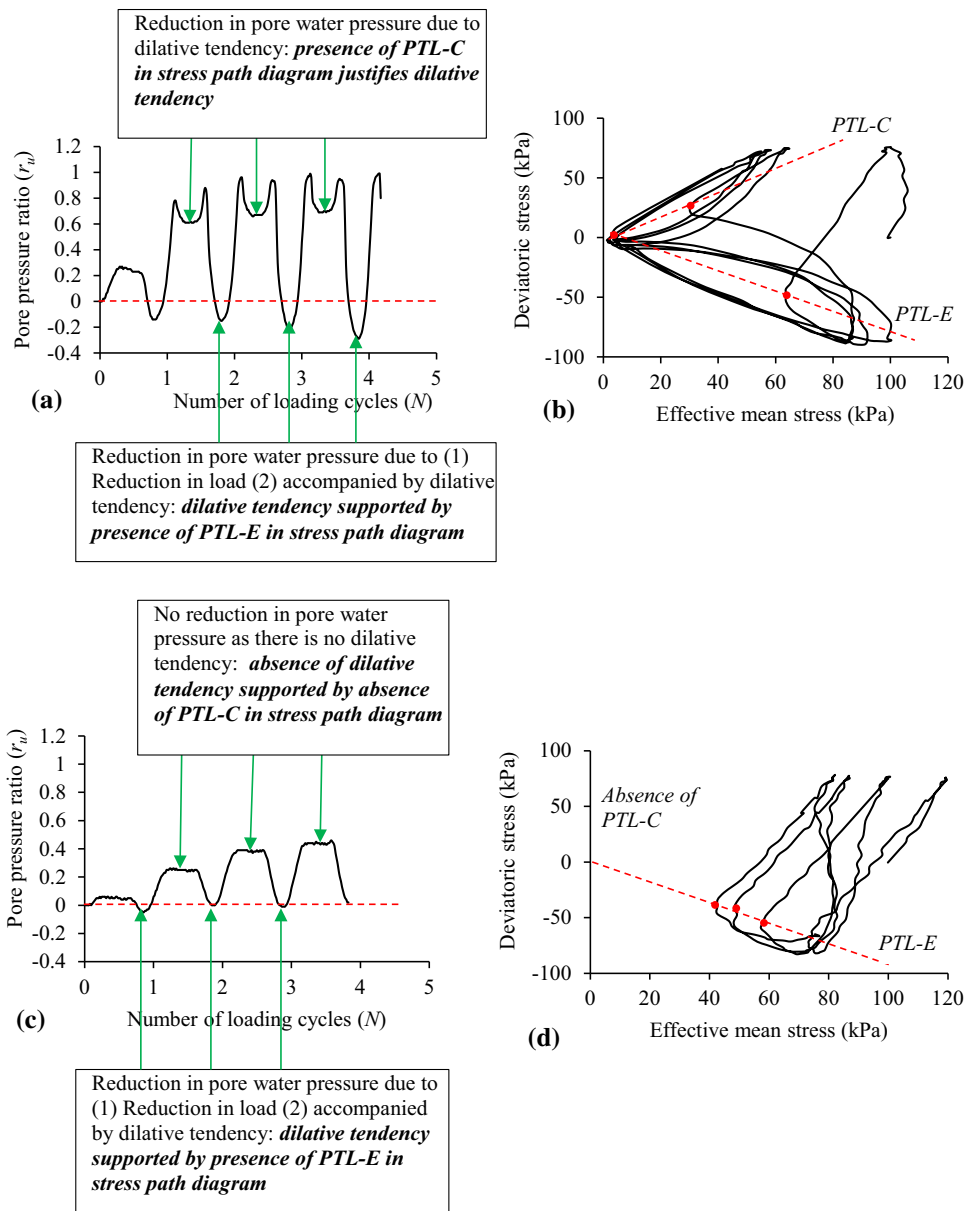
In FAPSCS-SS, the sample goes on accumulating axial strain on the compressions side gradually. The rate of accumulation of strain increases with the number loading cycles. This is due to a gradual reduction in soil stiffness. This gradual reduction in stiffness is called as strain

softening. However, this failure does not come under the category of liquefaction failure as it does not show sudden and large axial straining due to the generation of pore pressure which is observed in typical liquefaction failure.

Cyclic Mobility Versus Cyclic Softening

In both cyclic mobility and cyclic softening, deformations are large, but the cause and mechanism are different. In the

Fig. 17 Role of phase transformation line in identifying dilative tendency, CSR 0.4, D_r 60%: **a** pore pressure ratio evolution S 98.5%, **b** effective stress path S 98.5%, B 0.63, **c** pore pressure ratio evolution S 83.6%, **d** effective stress path S 83.6%, B 0.12



case of cyclic mobility, large strains are due to reaching a state of zero effective confining pressure, whereas in cyclic softening large strains are result of strain softening without reaching a state of zero effective confining pressure. It should be noted that in the case of cyclic mobility, sample undergoes phase transformation during both compression and extension stages of loading and deforms on both compression and extension sides, irrespective of relative density, confining pressure and CSR . In the case of cyclic softening, the sample undergoes deformation on the extension side only. Further, in cyclic softening, phase transformation can occur during both stages of loading or extension stage of loading only. Depending on the occurrence of phase transformation, cyclic softening has been categorized as (1) cyclic softening-CE, where sample

undergoes phase transformation during both compression and extension stage of loading as shown in Fig. 14 and (2) cyclic softening-E, where sample undergoes phase transformation during extension stage of loading only as shown in Fig. 16b. Further, in the case of cyclic softening-E, the sample undergoes unlimited flow at the end of loading, as shown in Fig. 18.

Factors Affecting Axial Strain Evolution Patterns: Symmetry/Asymmetry

Typical axial strain evolution patterns for five distinct failure modes are shown in Fig. 19. In cyclic mobility, axial strain evolution is symmetric, whereas in hybrid cyclic liquefaction strain, evolution is asymmetric and falls

Fig. 18 Comparison of stress–strain curves of various failure modes

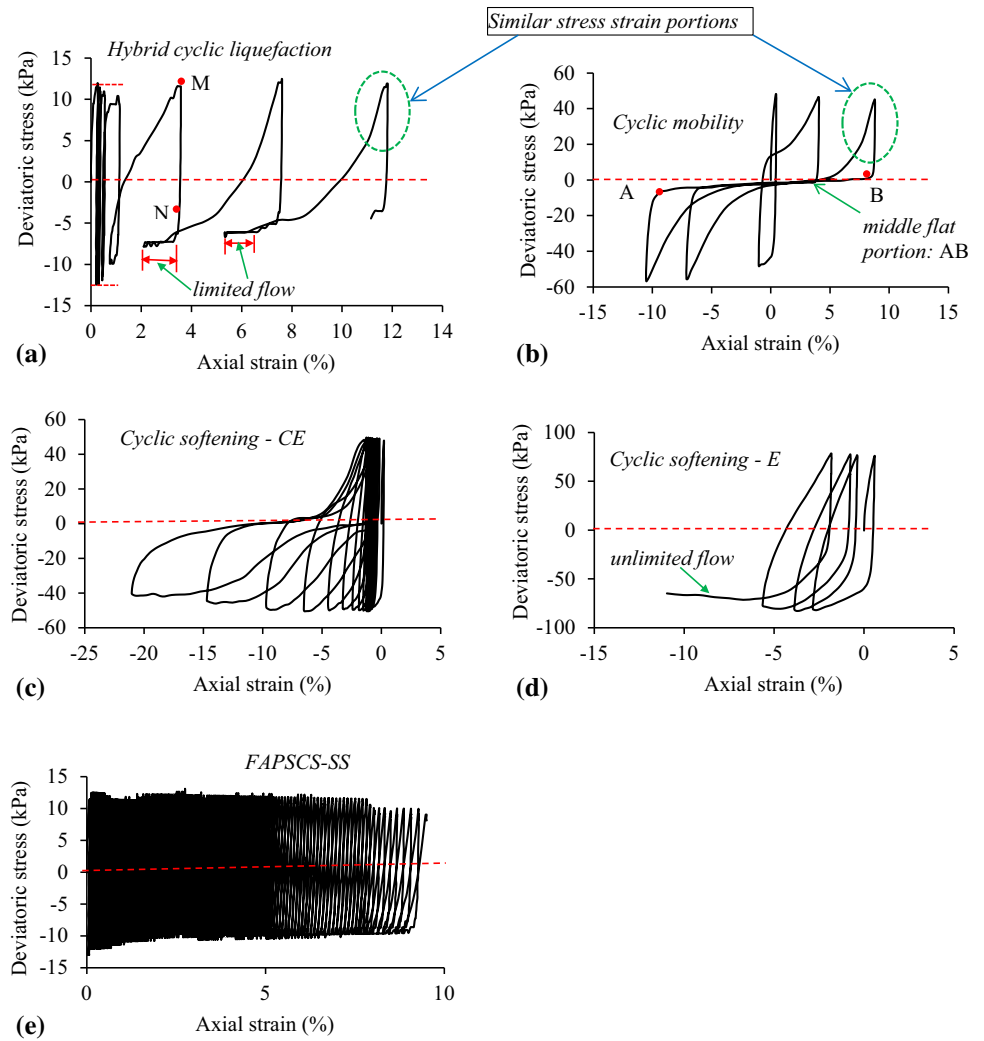
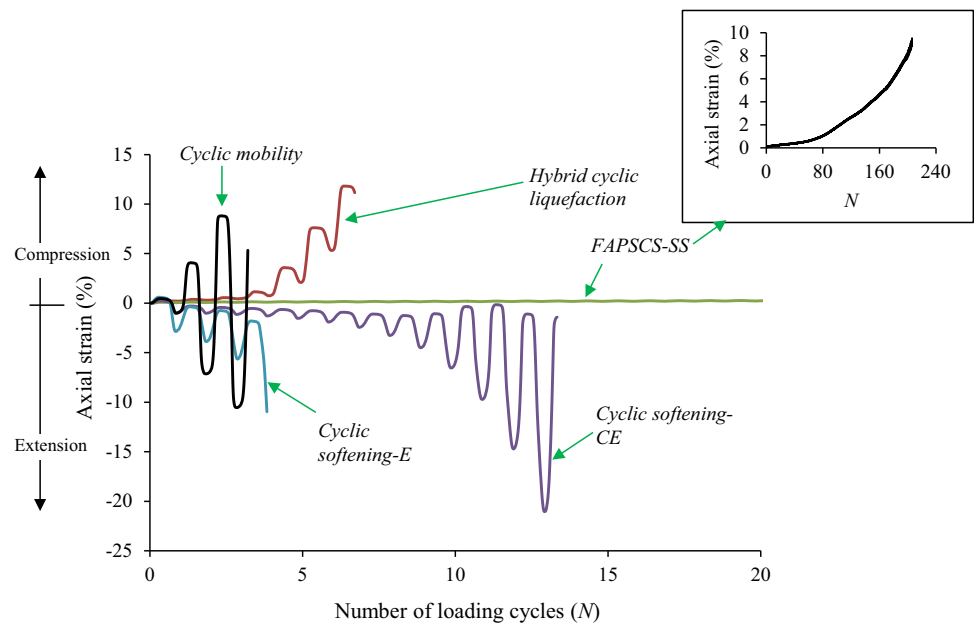


Fig. 19 Comparison of axial strain evolution patterns observed in various failure modes



on the compression side. Axial strain evolution of cyclic softening-CE and cyclic softening-E is also asymmetric, but it lies on the extension side. In the case of FAPSCS-SS asymmetric strain evolution on the compression side is observed. In this figure, the full axial strain evolution for FAPSCS-SS is shown in the inset and in the main figure strain evolution is only up to 20 cycles. This is because when full axial strain evolution for FAPSCS-SS, N around 200, is shown in the main figure, it suppresses the distinctiveness of rest four strain patterns. Strain evolution patterns observed in this study depend on: (1) degree of saturation S , (2) relative density D_r , (3) initial effective confining pressure σ'_c and (4) cyclic shear stress ratio (CSR). Thus, depending upon the above-mentioned four factors, air desaturated sand can undergo any of the following failures: (a) catastrophic cyclic mobility, (b) gradual cyclic mobility, (c) hybrid cyclic liquefaction, (d) cyclic softening-CE (e) cyclic softening-E and f) FAPSCS-SS.

Insight from Critical State Framework

In this section, failure modes have been investigated from the framework of critical state soil mechanics. For this purpose, first of all, a critical state line for sand used in this study has been established by conducting eight isotopically consolidated undrained compression (ICUC) triaxial tests and three isotopically consolidated drained compression (ICDC) triaxial tests. For brevity, results of the undrained triaxial tests only are shown in Fig. 20.

This approach is conventionally used to discuss the mechanical behaviour of soil under a drained or undrained condition wherein pore fluid is incompressible [27]. Therefore, the mechanical response of nearly saturated samples only is investigated as, in this case, pore fluid is almost incompressible due to the very small amount of air in the voids.

The critical state line in $q-p'$ space and $e-\log(p')$ space is shown in Fig. 21. The initial state of the nearly saturated samples of relative density of 30%, 40% and 60% at various initial effective confining pressures is shown in Fig. 21b. A well-established state parameter, $\psi = e - e_c$, has been used to define the initial state of the sample with respect to its critical state where e is the initial void ratio of the sample and e_c is the critical void ratio at the same effective mean stress [28]. ψ positive implies that e is greater than e_c ; in this case, initial state of the sample is said to be loose of critical. If ψ is negative, then e is less than e_c and the initial state of the sample is said to be dense of critical. From Fig. 21b, it is clear that the initial state of all tested samples falls on the dense side of the critical state line, i.e. ψ is negative. Moreover, it is observed from Fig. 21b that the sample closest to its critical state, ψ

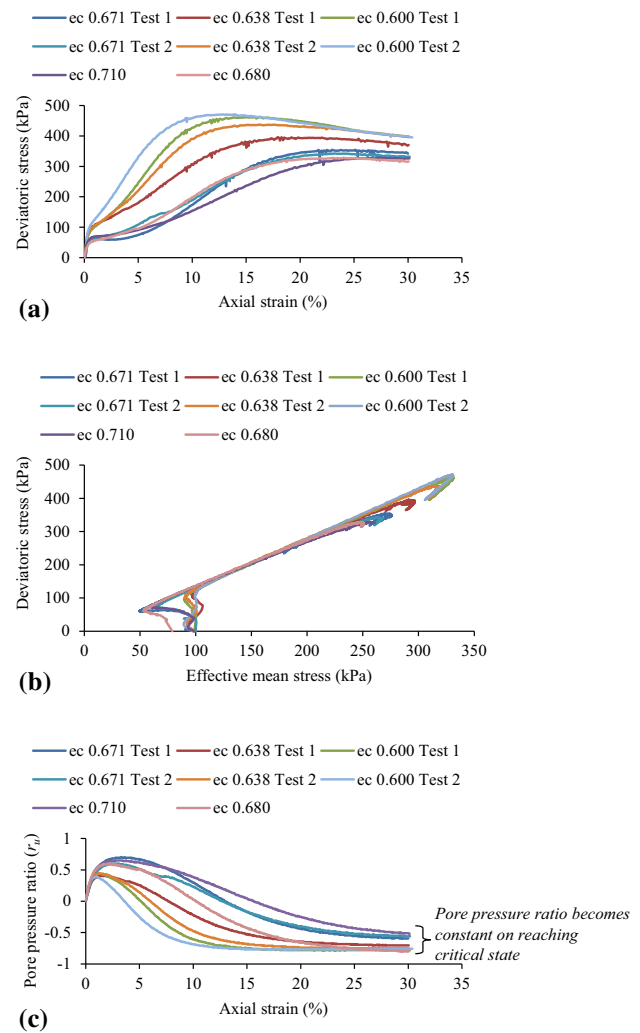


Fig. 20 Response of undrained static tests conducted to define critical state line: **a** stress–strain curves, **b** effective stress paths, **c** evolution of pore pressure ratio

– 0.036, undergoes catastrophic cyclic mobility failure, whereas the sample farthest from its critical state, ψ – 0.206, undergoes FAPSCS-SS failure. Samples at intermediate states undergo either hybrid cyclic liquefaction or gradual cyclic mobility.

Mechanism Behind Failure Modes and Role of State Parameter

Though the initial state of all samples falls on the dense side of the critical state line, failure modes observed are different, depending on the initial position of the sample with reference to the critical state. The mechanism behind different failure modes with respect to critical state can be understood in the following way: all samples lying on the dense of critical side undergoes: (1) initial contraction, followed by (2) dilation, in drained compression tests. The

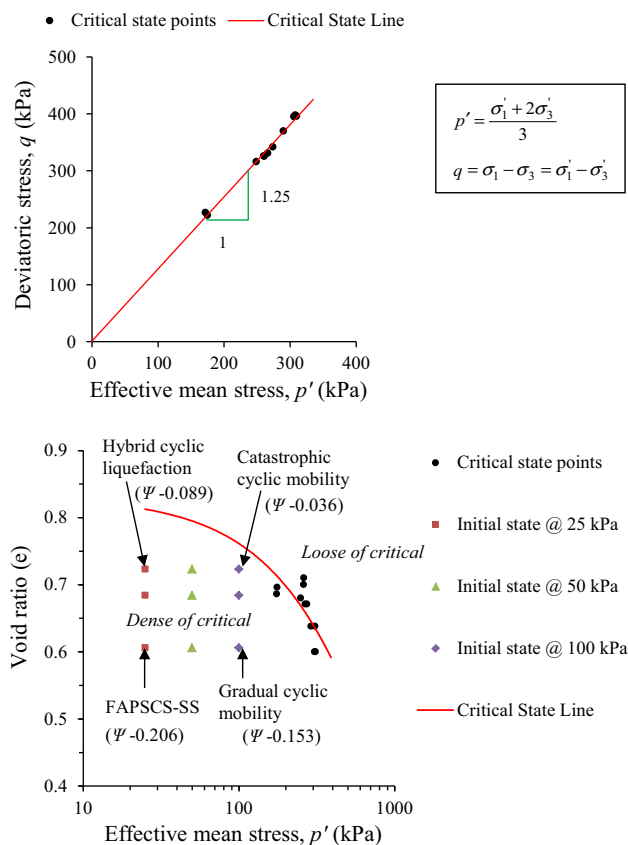


Fig. 21 Insight from critical state framework: **a** critical state line in q - p' space, **b** critical state line in e - $\log(p')$ space along with initial state of tested samples

same sample when subjected to undrained compression test shows: (1) initial contractive tendency, followed by (2) dilative tendency [29]. The contractive tendency is responsible for the generation of excess pore pressure, while the dilative tendency is responsible for the reduction in the excess pore pressure in undrained loading. In undrained cyclic loading, various failure modes are observed due to the combined effect of (1) contractive tendency, (2) dilative tendency and (3) nature of loading, which is cyclic. Sample closest to critical state, i.e. with $\psi = -0.036$, has a tendency to undergo contraction at a very fast rate, whereas sample farthest from critical state i.e. with $\psi = -0.206$, has a tendency to undergo contraction at an extremely slow rate. As the sample closest to its critical state tries to contract at a very fast rate; it generates very high excess pore pressure within the first few loading cycles only, due to which the sample undergoes very large axial straining. At the end of this, large axial straining dilative tendency comes into play and prevents the sample from undergoing unlimited flow. Under such conditions, catastrophic cyclic mobility is observed. Sample with $\psi = -0.089$ also generates very high excess pore pressure within the first few loading cycles only and undergoes

hybrid cyclic liquefaction. Samples at a relatively farther distance from critical state, i.e. say $\psi = -0.153$, has also an initial contractive tendency, but this happens at a relatively slow rate. In this case, the sample undergoes large axial straining but at a relatively large number of loading cycles. This results into gradual cyclic mobility. Sample farthest from critical state, i.e. $\psi = -0.206$, tries to contract at a very slow rate which results into FAPSC-SS failure. From the above discussion, it can be inferred that samples closer to critical state undergoes either catastrophic cyclic mobility or hybrid cyclic liquefaction, whereas that farther from it undergoes either gradual cyclic mobility or FAPSC-SS.

Does r_u of 1 Mean Liquefaction Failure?

It is observed that in the case of FAPSC-SS sample attains r_u of 1, but it does not undergo sudden and large axial straining which is observed in typical liquefaction failures. This is so because the generation of pore pressure, in this case, takes place at a very slow rate. This implies that just attaining r_u of 1 is not enough to cause the liquefaction failure, but it has to happen at a faster rate. Then only it results into sudden and large axial straining. In the literature, r_u of 1 is one of the most widely used liquefaction failure criteria [30, 31]. But from the present study, it is observed that r_u of 1 results into liquefaction failure only when it is attained at faster rate. Therefore, it is not just the magnitude of the pore water pressure, but the rate at which it is attained is also important.

Liquefaction Failure Criterion for Air Desaturated Sandy Soil

Pore pressure ratio (r_u) and double amplitude axial strain (DA) are the two most widely used parameters to define liquefaction failure of sandy soil [31]. In the pore pressure ratio criterion, the sample is considered to have failed once the pore pressure ratio (r_u) becomes 1. This condition of r_u equal to 1 is also called as initial liquefaction. In the case of the double amplitude axial strain (DA) criterion, failure is assumed to have occurred when the sample accumulates 5% double amplitude axial strain [3, 30].

In the present study, more than forty stress-controlled undrained cyclic triaxial tests have been conducted, and the types of failure observed at various initial effective confining pressure, relative density, degree of saturation and CSR, are mentioned in Table 2. From this study, it is found that nearly saturated samples attains a state of initial liquefaction and undergoes large axial deformations. However, desaturated samples at a low degree of saturation undergo large axial deformation without reaching a state of initial liquefaction. Defining liquefaction failure on the basis of initial liquefaction can be misleading in the case of

Table 2 Failure modes observed for samples of different relative density, initial effective confining pressure and degree of saturation

Sr. No	D_r %	σ'_c (kPa)	B	S %	Failure mode
1	30	25	0.70	98.5	Hybrid cyclic liquefaction
2		25	0.40	95.1	Hybrid cyclic liquefaction
3		25	0.37	94.3	Hybrid cyclic liquefaction
4		25	0.21	87.2	Hybrid cyclic liquefaction
5		50	0.70	98.5	Cyclic mobility
6		50	0.40	95.1	Cyclic mobility
7		50	0.29	91.9	Cyclic mobility
8		50	0.19	86.6	Cyclic mobility
9		100	0.70	98.5	Cyclic mobility
10		100	0.38	94.4	Cyclic mobility
11		100	0.23	89.2	Cyclic mobility
12		100	0.11	74.0	Cyclic softening-CE
13	40	25	0.65	98.5	Hybrid cyclic liquefaction
14		25	0.57	98.0	Hybrid cyclic liquefaction
15		25	0.50	97.3	Hybrid cyclic liquefaction
16		25	0.48	97.1	Hybrid cyclic liquefaction
17		25	0.20	90.0	Hybrid cyclic liquefaction
18		50	0.65	98.5	Cyclic mobility
19		50	0.23	91.5	Cyclic mobility
20		50	0.13	82.2	Cyclic mobility
21		50	0.08	69.2	Cyclic mobility
22		100	0.65	98.5	Cyclic mobility
23		100	0.48	97.1	Cyclic mobility
24		100	0.19	89.5	Cyclic mobility
25		100	0.12	81.4	Cyclic mobility
26		100	0.11	79.2	Cyclic mobility
27		100	0.07	68.4	Cyclic softening-CE
28	60	25	0.63	98.5	FAPSCS-SS
29		25	0.32	94.9	NF, NL 258
30		50	0.63	98.5	Cyclic mobility
31		50	0.56	98.1	Cyclic mobility
32		50	0.41	96.5	Cyclic mobility,
33		50	0.21	91.4	NF, NL 250
34		100	0.63	98.5	Cyclic mobility, CSR 0.4
35		100	0.52	97.7	Cyclic mobility, CSR 0.4
36		100	0.22	91.9	Cyclic mobility, CSR 0.4
37		100	0.12	83.6	Cyclic softening-E, CSR 0.4
38		100	0.63	98.5	Cyclic mobility
39		100	0.56	98.1	Cyclic mobility
40		100	0.54	97.9	Cyclic mobility
41		100	0.53	97.8	Cyclic mobility
42		100	0.28	94.0	Cyclic mobility
43		100	0.22	91.9	Cyclic mobility
44		100	0.11	82.1	NF, NL 202

FAPSCS-SS failure due to accumulation of plastic strain on compression side as a result of gradual strain softening; NF sample does not undergo any of the abovementioned failures, NL total number of loading cycles

desaturated samples at a low degree of saturation. Therefore, it is recommended from this study that the double amplitude axial strain (DA) criterion [3] should be used as a liquefaction failure criterion in case of air desaturation.

Conclusions

In this study, large number of undrained cyclic triaxial tests have been carried out to explore failure modes observed in air desaturated sandy soil over a wide range of degrees of saturation. The effect of relative density, effective confining pressure and *CSR*, on the failure modes, has also been investigated. Major findings from the present study are summarized below:

1. Hybrid cyclic liquefaction was observed at low initial effective confining pressure for samples of loose sand with a degree of saturation varying from 99% to around 90%. This type of failure comprised, up to some extent, the response of cyclic mobility and limited flow. However, nearly saturated sample of medium dense sand at low initial effective confining pressure failed due to the accumulation of plastic strain on the compression side as a result of gradual strain softening.
2. At low effective confining pressure, for a sample of relative density of 30%, axial strain evolution comprised two distinct regions. Over the first region, called as low rate region, axial strain evolved at a very slow rate, whereas over the second region, called as high rate region, axial strain evolved at a significantly higher rate. It was the pore pressure ratio (r_u) which defined the transition from LR to HR. The transition pore pressure ratio was found to be around 0.6.
3. At high initial effective confining pressure, samples with degree of saturation spanning from 99% to around 90% underwent cyclic mobility failure irrespective of the relative density.
4. The cyclic mobility observed in a nearly saturated sample of loose sand is catastrophic in comparison with that observed in medium dense sand. This implies that during undrained cyclic loading, generation of even a very small pore pressure ratio of 0.1 can be alarming for loose sand, whereas at the same pore pressure ratio medium dense sand can be quite stable.
5. Sample with S 98.5% (D_r 60%, σ'_c 100 kPa, CSR 0.4) showed phase transformation during compression stage of loading, whereas it was absent in sample with S 83.6%. Moreover, large negative pore water pressure was developed in the nearly saturated sample during the extension stage of loading due to high dilative tendency. On the other hand, sample with S 83.6% generated very small negative pore water pressure during the extension stage of loading due to low dilative tendency. Thus, it was observed that the presence of air in desaturated sand affects both dilative tendency and phase transformation.
6. Phase transformation line plays a vital role in identifying whether the reduction in pore water pressure during the extension stage is due to a reduction in axial stress and/or the dilative tendency of the sample. Pore pressure evolution plot only is not enough to identify this. The pore pressure plot and effective stress path together give information regarding reduction in pore pressure owing to dilative tendency.
7. At low degree of saturation, cyclic softening-CE and cyclic softening-E were observed, depending upon relative density and CSR . These two failures are demarcated by two distinct phase transformation trends observed during failure.
8. In both cyclic mobility and cyclic softening, deformation is large; however, the cause and mechanism are different. In cyclic mobility, large strains are due to reaching a state of zero effective confining pressure, whereas in cyclic softening large strains are the result of a reduction in the stiffness without reaching a state of zero effective confining pressure. A middle flat portion representing almost zero stiffness is observed in stress–strain curve of cyclic mobility failure, whereas it is absent in stress–strain curve for cyclic softening.
9. It was observed that sudden and large axial straining indicating typical liquefaction failure occurs only when pore pressure increases at a sufficiently high rate and eventually becomes equal to the initial effective confining pressure.
10. Strain evolution patterns observed in the case of air desaturated sandy soil depend on: (1) degree of saturation S , (2) relative density D_r , (3) initial effective confining pressure σ'_c and (4) cyclic shear stress ratio (CSR). Depending on the above-mentioned four factors, air desaturated sand can undergo any of the following failures: (a) catastrophic cyclic mobility, (b) gradual cyclic mobility, (c) hybrid cyclic liquefaction, (d) cyclic softening-CE, (e) cyclic softening-E, (f) FAPSCS-SS and (g) a failure which is a transition from hybrid cyclic liquefaction to cyclic mobility.
11. Insight from critical state framework revealed that nearly saturated sample closest to critical state undergoes catastrophic cyclic mobility failure, whereas sample farthest from its critical state

undergoes FAPSCS-SS failure. Samples at intermediate states undergo either hybrid cyclic liquefaction or gradual cyclic mobility.

12. It is recommended from the present study that double amplitude axial strain (DA) should be used as a liquefaction failure criterion for air desaturated sandy soil.

Funding No funding was received for conducting this study.

Declarations

Conflict of interest The authors declare that they have no conflict of interest.

References

1. Castro G (1969) Liquefaction of sands. Harvard University, Cambridge Massachusetts
2. Ishihara K (1993) Liquefaction and flow failure during earthquakes. *Geotechnique* 43:351–415
3. Ishihara K (1996) Soil behaviour in earthquake geotechnics. Oxford Science Publications, Oxford
4. Kramer SL (1996) Geotechnical earthquake engineering. Pearson, New York
5. Idriss IM, Boulanger R (2008) Soil liquefaction during earthquakes. EERI
6. Sze HY, Yang J (2014) Failure modes of sand in undrained cyclic loading: impact of sample preparation. *Geotech Geoenviron Eng*. [https://doi.org/10.1061/\(ASCE\)GT.1943-5606.0000971](https://doi.org/10.1061/(ASCE)GT.1943-5606.0000971)
7. Ishihara M, Okamura M, Oshita T (2003) Desaturating sand deposit by air injection for reducing liquefaction potential. In: Pacific Conference on Earthquake Engineering
8. Pietruszczak S, Pande GN, Oulapour M (2003) A hypothesis for mitigation of risk of liquefaction. *Géotechnique* 53:833–838. <https://doi.org/10.1680/geot.2003.53.9.833>
9. Yegian MK, Eseller-Bayat E, Alshawabkeh A, Ali S (2007) Induced-partial saturation for liquefaction mitigation: experimental investigation. *J Geotech Geoenviron Eng* 133:372–380. [https://doi.org/10.1061/\(ASCE\)1090-0241\(2007\)133:4\(372\)](https://doi.org/10.1061/(ASCE)1090-0241(2007)133:4(372))
10. Takemura J, Igarashi R, Izawa J, Okamura M, Masuda M (2009) Centrifuge model tests on soil desaturation as a liquefaction countermeasure. *Proc Int Conf Soil Mech Geotech Eng Acad Pract Geotech Eng* 1:502–505. <https://doi.org/10.3233/978-1-60750-031-5-502>
11. Marasini NP, Okamura M (2015) Numerical simulation of centrifuge tests to evaluate the performance of desaturation by air injection on liquefiable foundation soil of light structures. *Soils Found* 55:1388–1399. <https://doi.org/10.1016/j.sandf.2015.10.005>
12. Zeybek A, Madabhushi SPG (2016) Centrifuge testing to evaluate the liquefaction response of air-injected partially saturated soils beneath shallow foundations. *Bull Earthq Eng*. <https://doi.org/10.1007/s10518-016-9968-6>
13. Okamura M, Takebayashi M, Nishida K, Fujii N, Jinguji M, Imasato T et al (2011) In-Situ desaturation test by air injection and its evaluation through field monitoring and multiphase flow simulation. *J Geotech Geoenviron Eng* 137:643–652. [https://doi.org/10.1061/\(ASCE\)GT.1943-5606.0000483](https://doi.org/10.1061/(ASCE)GT.1943-5606.0000483)
14. He J, Chu J, Ivanov V (2013) Mitigation of liquefaction of saturated sand using biogas. *Géotechnique* 63:267–275. <https://doi.org/10.1680/geot.SIP13.P.004>
15. Zeybek A, Madabhushi SPG (2017) Influence of air injection on the liquefaction-induced deformation mechanisms beneath shallow foundations. *Soil Dyn Earthq Eng* 97:266–276. <https://doi.org/10.1016/j.soildyn.2017.03.018>
16. Marasini NP, Okamura M (2015) Air injection to mitigate liquefaction under light structures. *Int J Phys Model Geotech* 15:129–140. <https://doi.org/10.1680/jphmg.14.00005>
17. He J, Chu J (2014) Undrained responses of microbially desaturated sand under monotonic loading. *J Geotech Geoenviron Eng* 140:04014003. [https://doi.org/10.1061/\(ASCE\)GT.1943-5606.001082](https://doi.org/10.1061/(ASCE)GT.1943-5606.001082)
18. IS: 2720 (Part 4) – 1985 (2006) (Reaffirmed 2006)
19. IS: 2720 (Part 3/Sec 1) - 1980 (2002) (Reaffirmed 2002)
20. IS: 2720 (Part 14) -1983 (2006) (Reaffirmed 2006)
21. Xin L, Jun Y, Gonghui W, Longzhu C (2016) Small-strain shear modulus of volcanic granular soil: an experimental investigation. *Soil Dyn Earthq Eng* 86:15–24
22. Black D, Lee K (1973) Saturating laboratory samples by back pressure. *J Soil Mech Found Div* 99:75–95
23. Skempton AW (1954) The pore-pressure coefficients A and B. *Géotechnique* 4:143–147. <https://doi.org/10.1680/geot.1954.4.4.143>
24. Yoshimi Y, Tanaka K, Tokimatsu K (1989) Liquefaction resistance of a partially saturated sand. *Soils Found* 29:157–162
25. Celestino V, Kenneth H (2012) Seismic measurements in sand specimens with varying degrees of saturation using piezoelectric transducers. *Can Geotech J* 68:671–685. <https://doi.org/10.1139/T2012-033>
26. Lade PV (2016) Triaxial Testing of Soils, 1st edn. John Wiley and Sons Ltd, New York
27. Schofield A, Wroth P (1968) Critical state soil mechanics. McGraw-hill, London
28. Been K, Jefferies MG (1985) A state parameter for sands. *Géotechnique* 35:99–112
29. Salgado R (2008) The engineering of foundations. McGraw-Hill Higher Education, New York
30. Poulos SJ, Castro G, France JW (1985) Liquefaction evaluation procedure. *J Geotech Geoenviron Eng* 111:772–792
31. Boulanger RW, Idriss IM (2006) Liquefaction susceptibility criteria for silts and clays. *J Geotech Geoenviron Eng* 132:1413–1426

Publisher's Note Springer Nature remains neutral with regard to jurisdictional claims in published maps and institutional affiliations.